3

Vehicle Modeling

Lowell Brown and Dustin Edwards

3.1 Introduction

The goal of any model is to describe physical phenomena. Our interest is vehicular dynamics. There are several models that exist for describing vehicle motion [1–16]. We will explore a few of them. First, though, conventions must be established.

3.2 SAE Vehicle Coordinates

The Society of Automotive Engineers has established the SAE Vehicle Coordinate System. This is the system that will be used for body fixed coordinates. As shown in Figure 3.1 this coordinate system defines the longitudinal axis of the vehicle as x, the lateral axis to be y, and the vertical axis, z, points toward the ground. The coordinate system also defines the direction of roll rate p, pitch rate q, and yaw rate r.

The body fixed SAE coordinate systems is attached to a vehicle that moves about the East, North, Up (ENU) global reference frame, as shown in Figure 3.2.

In Figure 3.2 the horizontal axis is the East direction and vertical axis is the North direction. The positive Up direction comes out pointed at the

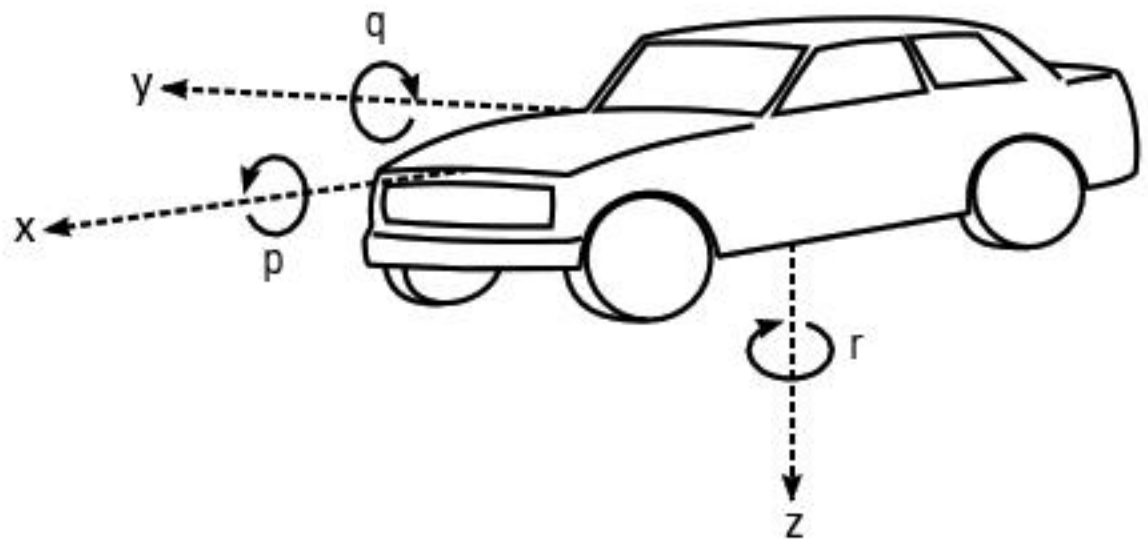

Figure 3.1 SAE Vehicle Coordinate System defined by the SAE [1].

reader and is perpendicular to the E-N plane. The box represents a vehicle with V_x and V_y velocity components. Vehicle heading is ψ, the angle between a line parallel to the North axis and the longitudinal velocity component V_x. Sideslip, β, is defined as the angle between the magnitude of velocity and the longitudinal component of velocity, V_x. Vehicle course, the direction of travel, is defined as ν, where

$$\nu = \psi + \beta \tag{3.1}$$

Note that ψ is equivalent to r, the yaw rate.

Most models in this chapter will be based off the basic "bicycle model." Other models are developed to capture dynamics the bicycle model is unable to describe. Also, simplifications are made to the bicycle model that are valid

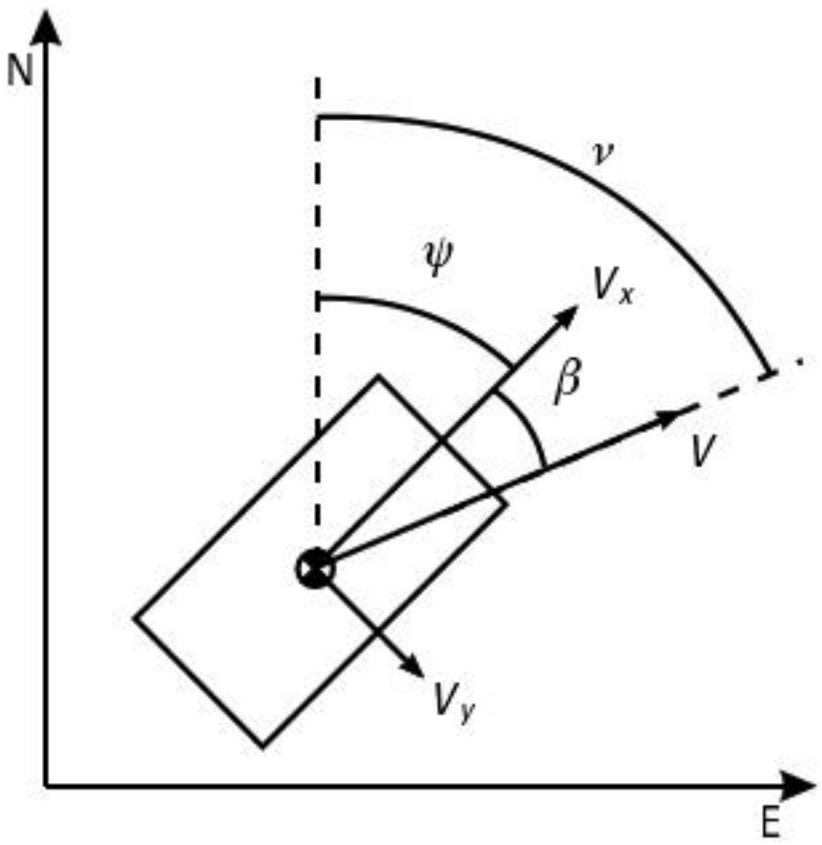

Figure 3.2 ENU global reference plane.

during certain steady-state maneuvers. The models developed in this chapter are important in later sections when developing parameter estimation algorithms and controlling a vehicle autonomously. Therefore, it is important to know the limitations and accuracy of each model.

3.3 Bicycle Model

3.3.1 Basics

3.3.1.1 Assumptions

Now that coordinate conventions have been established, the vehicle models can be explored. The first of these models is the bicycle model. In the bicycle model the inner and outer tires of each axle are represented by a single tire at the center of the vehicle's axle. Thus the front is represented by a single front tire and the rear axle is represented by a single rear tire. So, the assumption is made that the inner and outer slip angles and the inner and outer steer angles are the same. The steering angle of the vehicle is represented by δ. The slip angle of the vehicle is denoted as β and describes the angle between the velocity vector and the longitudinal axis of the vehicle. The bicycle model also neglects weight transfer, the difference in vertical force between the inner and outer tires.

Figure 3.3 represents the bicycle model. The CG is the center of gravity. The body fixed reference frame has an origin at the vehicle's center of gravity. The z-axis is pointing down toward the ground, the x-axis is pointing toward the front of the vehicle, and the y-axis is pointing out to the vehicle's passenger side. In Figure 3.3, δ is the steering angle, and a and b are distances

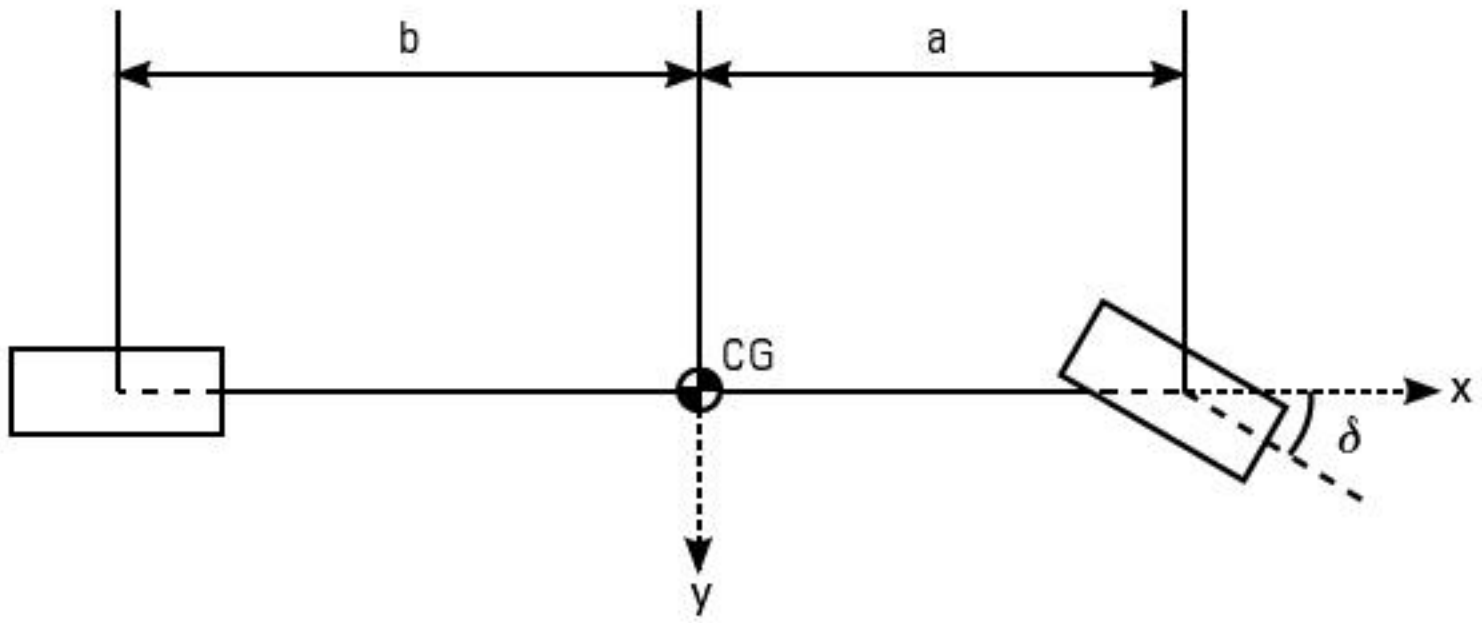

Figure 3.3 Bicycle model.

from the vehicle center of gravity to the front and rear axles, respectively. This model assumes that left and right steer angles are the same for front and rear axles.

3.3.1.2 Kinematic Version

At low speeds with no slip or minimal slip, the slip angles at the tires can be assumed to be zero, which produces the lateral kinematic version of the bicycle model. The perpendicular line from each tire passes through the same point, which is called the center of the turn. Figure 3.4 represents the kinematic bicycle model. Note the perpendicular lines that originate at each axle and pass through the center of the radius, R. If the steering angle of the front tire reaches zero, the radius of curvature, R, goes to infinity. When the steering angle is not zero the steering angle can be described by (3.2), known as the Ackerman angle.

$$\delta = \tan^{1} \frac{L}{R} \div \frac{L}{R} \tag{3.2}$$

By using simple kinematics, the vehicle's velocity, V, can be described as the yaw rate, r, of the vehicle times the radius of curvature, R. Also with no lateral sliding, the lateral acceleration, a_y, of the vehicle is simply the centripetal acceleration developed during the turn.

$$V = Rr \tag{3.3}$$

$$a_y = \dot{V}_y = Rr^2 = \frac{V^2}{R} = Vr \tag{3.4}$$

Substituting (3.3) into (3.2) results in the expected yaw rate of the kinematic model, given a steer input and velocity.

$$r = \frac{V}{L} \div \tan(\delta) \quad \frac{V}{L} \div \delta \tag{3.5}$$

3.3.1.3 Lateral Version

For higher speeds that develop greater slip angles the lateral bicycle model can be used for vehicles that produce minimal roll angles. Figure 3.5 represents the lateral bicycle model where r is the yaw rate, $V = [V_x \ \ Y_y]_T$ is the velocity vector acting at the vehicle's center of gravity, b represents the sideslip angle, d is the steering angle, and a and b are distances from the vehicle center of

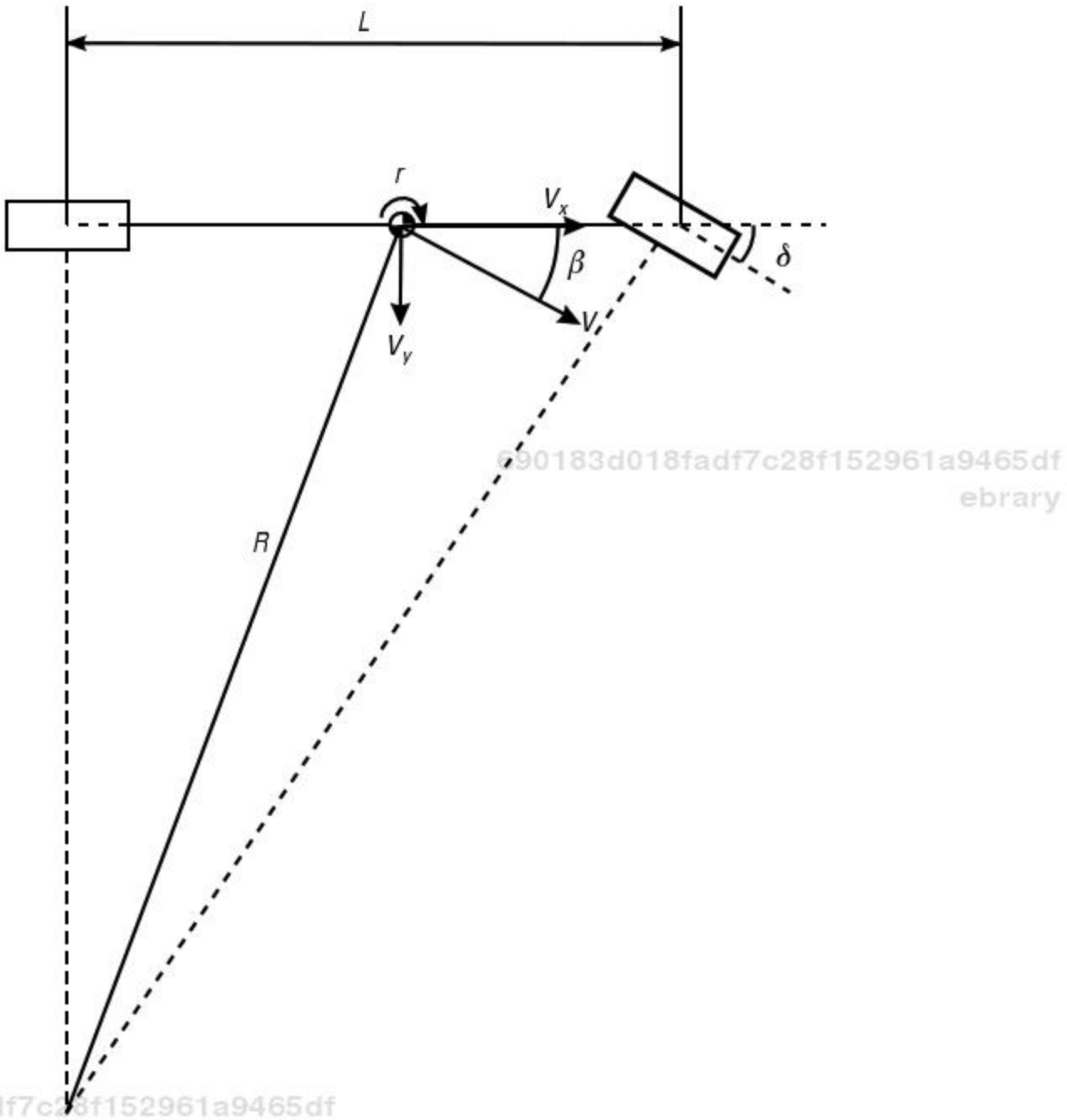

Figure 3.4 Kinematic bicycle model.

gravity to the front and rear axles, respectively. The front and rear tire slip angles are denoted as α_f and α_r, respectively. By summing the forces and moments about the CG on the free body diagram, Figure 3.5, and accounting for bank angle a simple set of dynamic equations can be derived to describe the vehicle's lateral motion. Note that the force due to the bank angle will be the mass times gravity times the sin of the bank angle.

$$F_y = m\ddot{y} = m(V_x\dot{\beta} + V_x r) = F_{yF} + F_{yR} + mgsin(\theta_{bank}) \tag{3.6}$$

$$M = I_z\ddot{\psi} = I_z\dot{r} = aF_{yF} + bF_{yR} \tag{3.7}$$

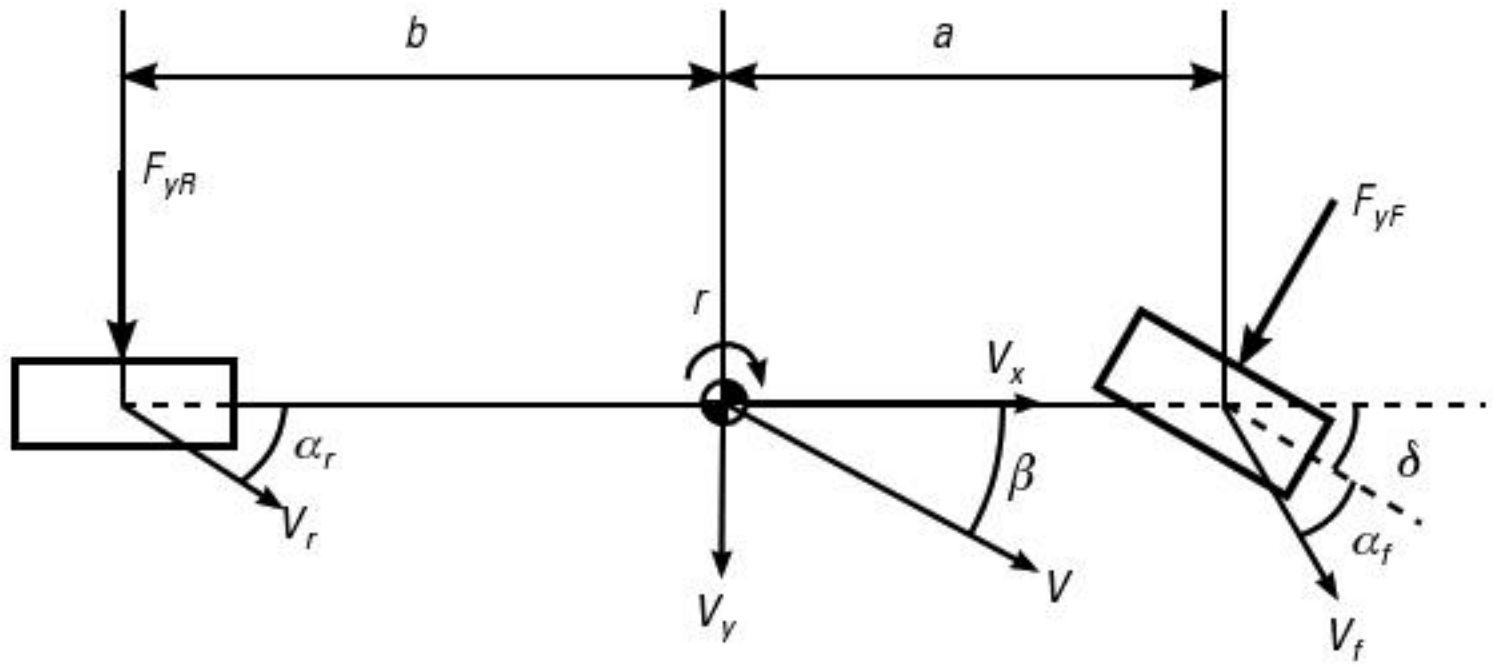

Figure 3.5 Lateral bicycle model.

Solving (3.6) and (3.7) for sideslip rate $\dot{\beta}$ and yaw acceleration $\dot{r}$ yields

$$\dot{\beta} = \frac{F_{yF}\cos(\delta) + F_{yR} + mgsin(\theta_{bank})}{mV_x} \quad r \tag{3.8}$$

$$\dot{r} = \frac{aF_{yF}\cos(\delta) \quad bF_{yR}}{I_z} \tag{3.9}$$

To describe the front and rear tire forces, $F_{yF,R}$, a linear tire model will be used. This model assumes the tire forces remain in the linear region of the tire and are proportional to the tire's respective slip angle times the tire's cornering stiffness, C_α, shown in (3.10) and (3.11). Tire models while be discussed more in depth in Section 3.4.3.

$$F_{yF} = \quad C_{\alpha f}\alpha_f \tag{3.10}$$

$$F_{yR} = \quad C_{\alpha r}\alpha_r \tag{3.11}$$

Substituting (3.10) and (3.11) into (3.6) and (3.7), a state space representation of this model can be developed and is shown by (3.12).

$$\begin{matrix} a_y \\ \dot{r} \end{matrix} = \begin{matrix} \frac{C_0}{mV_x} & V_x & \frac{C_1}{mV_x} & V_y \\ \frac{C_1}{I_zV_x} & & \frac{C_2}{I_zV_x} & r \end{matrix} + \begin{matrix} \frac{C_{\alpha f}}{m} \\ \frac{C_{\alpha f}a}{I_z} \end{matrix} \delta \tag{3.12}$$

where

$$C_0 = C_{\alpha f} + C_{\alpha r}$$
$$C_1 = aC_{\alpha f} \quad bC_{\alpha r} \tag{3.13}$$
$$C_2 = a^2 C_{\alpha f} + b^2 C_{\alpha r}$$

With a state space representation, this model can be configured for control or estimation purposes. Control and estimation are discussed in proceeding chapters.

Further examination of the lateral bicycle model can reveal the steady-state tire slip. Assuming yaw acceleration is equal to zero and lateral acceleration is equal to (3.4), the centripetal acceleration, then (3.6) and (3.7) are simplified.

$$m\frac{V_x^2}{R} = F_{yF} + F_{yR} \tag{3.14}$$

$$0 = aF_{yF} + bF_{yR} \tag{3.15}$$

Substituting (3.10) and (3.11) into the above equations, the steady-state tire slip can be solved.

$$\alpha_f = \frac{W_f V_x^2}{C_{\alpha f} gR} \tag{3.16}$$

$$\alpha_r = \frac{W_r V_x^2}{C_{\alpha r} gR} \tag{3.17}$$

For control purposes it is advantageous to look at the relationship between yaw rate, r, and steer angle, δ, or between sideslip, β, and steer angle, δ. Combining (3.10) and (3.11) into (3.6) and (3.7) in an alternate manner and again neglecting the bank angle yields the state space representation:

$$\begin{bmatrix} \dot{\beta} \\ \dot{r} \end{bmatrix} = \begin{bmatrix} \frac{C_0}{mV_x} & \frac{C_1}{mV_x^2} - 1 \\ \frac{C_1}{I_z} & \frac{C_2}{I_z V_x} \end{bmatrix} \begin{bmatrix} \beta \\ r \end{bmatrix} + \begin{bmatrix} \frac{C_{\alpha f}}{mV_x} \\ \frac{C_{\alpha f} a}{I_z} \end{bmatrix} \delta \tag{3.18}$$

The equations for the transfer function from steer angle to yaw rate and from steer angle to sideslip are shown here.

$$\frac{r(s)}{\delta(s)} = \frac{\frac{aC_{\alpha f}}{I_z}s + \frac{(a+b)C_{\alpha f}C_{\alpha r}}{mV_xI_z}}{s^2 + \frac{C_0I_z + mC_2}{mV_xI_z}s + \frac{C_0C_2 \quad C_1mV_x^2 \quad C_1^2}{mV_x^2I_z}} \tag{3.19}$$

$$\frac{\beta(s)}{\delta(s)} = \frac{\frac{C_{\alpha f}}{mV_x}s + \frac{C_{\alpha f}C_2 \quad aC_{\alpha f}C_1 \quad mV_x^2aC_{\alpha f}}{mV_x^2I_z}}{s^2 + \frac{C_0I_z + mC_2}{mV_xI_z}s + \frac{C_0C_2 \quad C_1mV_x^2 \quad C_1^2}{mV_x^2I_z}} \tag{3.20}$$

3.3.1.4 Longitudinal Dynamics

The longitudinal dynamics of a vehicle are influenced by the longitudinal force of the tires. Tires cannot generate force without slipping. This will be discussed in greater detail in Section 3.4.2. In order for a vehicle to move longitudinally slip must occur at the wheels. The percent slip of a wheel is a function of the velocity, V, angular velocity, ω, and effective radius, R_e, of the wheel and is defined as

$$\%\ \text{slip} = \frac{V \quad R_e\omega}{V} \tag{3.21}$$

The effective radius can be defined approximately as a function of the loaded radius, R_L, and the unloaded radius, R_U, of the wheel.

$$R_e \quad R_U \quad \frac{R_U \quad R_L}{3} \tag{3.22}$$

Examining the x-z plane of the SAE coordinate system and using a half car model generates the free body diagram (Figure 3.6). The effect of drag is modeled as ρV^2 acting on the CG where V is equivalent to $\dot{x}$ and the longitudinal velocity ρ is the drag coefficient. Note that wind speed is not taken into account. Also, note that the four wheels are combined into front and rear axles.

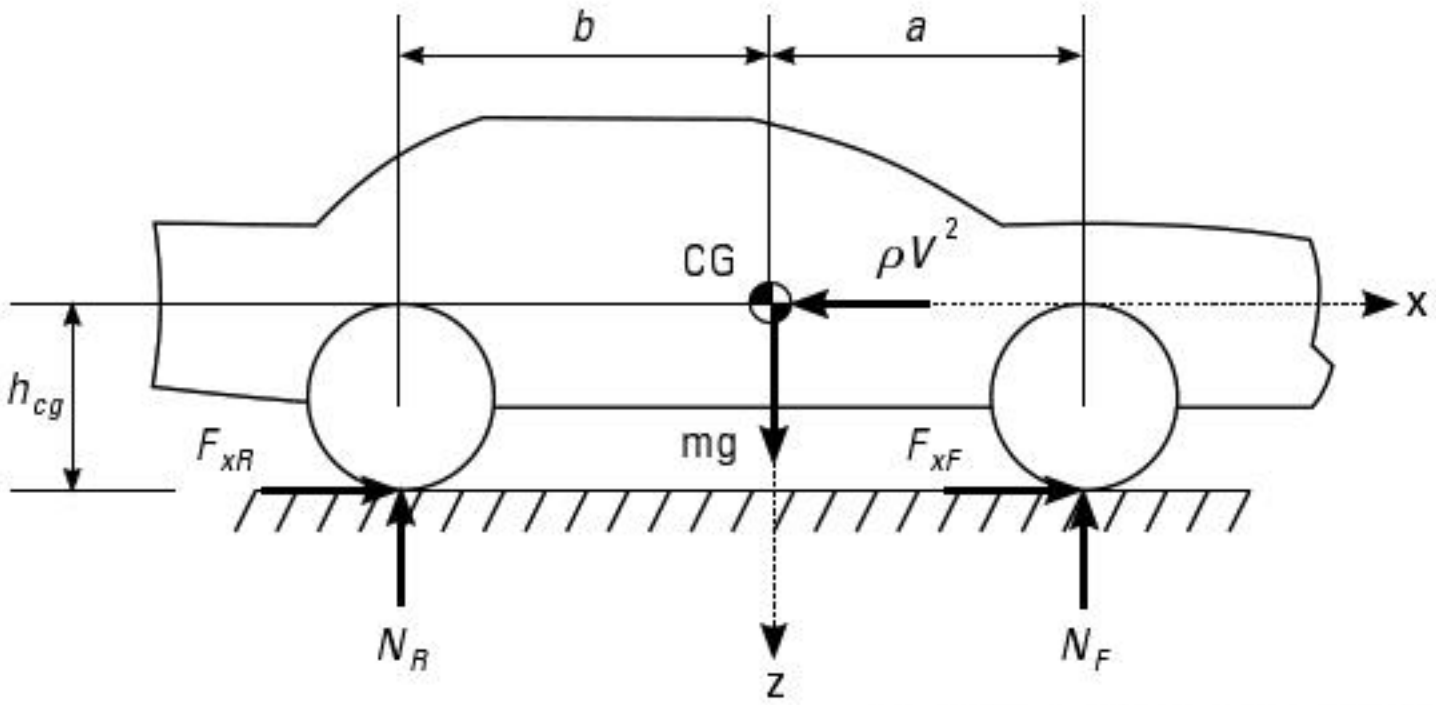

Figure 3.6 Longitudinal free body diagram.

Neglecting air drag and summing the forces and moments yields the longitudinal equations of motion.

$$F_z = m\ddot{z} = \quad N_F \quad N_R = mg \tag{3.23}$$

$$F_z = m\ddot{x} = F_{xF} + F_{xR} \tag{3.24}$$

$$M_{y,cg} = I_y\ddot{\theta} = bN_R \quad h_{cg}(F_{xF} + F_{xR}) \quad aN_F \tag{3.25}$$

 Combining the equations of motion produces solutions for the normal forces acting on the front and rear axles.

$$N_F = mg \quad \frac{I_y\theta + h_{cg}m\ddot{x} + amg \quad am\ddot{z}}{a+b} \quad M\ddot{z} \tag{3.26}$$

$$N_R = \frac{I_y\ddot{\theta} + h_{cg}m\ddot{x} + amg \quad am\ddot{z}}{a+b} \tag{3.27}$$

For the case of steady state pitch $\ddot{\theta} = 0$ and $\ddot{z} = g$. The normal forces on the front and rear axles then become

$$N_F = \frac{bmg}{a+b} \quad \frac{m\ddot{x}h_{cg}}{a+b} \tag{3.28}$$

$$N_R = \frac{amg}{a+b} + \frac{m\ddot{x}h_{cg}}{a+b} \tag{3.29}$$

Note that in the steady state pitch case the first term of N_F and N_R is the front and rear weight splits, respectively.

For the case with air drag included, the summation of forces in the x-direction becomes

$$F_x = m\ddot{x} = F_{xF} + F_{xR} \quad \rho\dot{x}^2 \tag{3.30}$$

The effect of air drag is important when designing a velocity controller. The control gains can be linearized about the operating point. This will be discussed in Chapter 6.

3.3.2 Understeer Gradient

In order to develop a better understanding of the turning response of a vehicle, the understeer gradient of the vehicle is defined. Using the steady-state bicycle model, the understeer gradient can be determined from the weight distribution and the cornering stiffness [8]. By including slip angles, a simple kinematic equation between the steer angle and tire slip angles can be developed.

$$\delta \quad \frac{L}{R} + \alpha_f \quad \alpha_r \tag{3.31}$$

Substituting (3.16) and (3.17) into (3.31) gives:

$$\delta \quad \frac{L}{R} + \quad \frac{W_f}{C_{\alpha f}} \quad \frac{W_r}{C_{\alpha r}} \div \frac{V^2}{gR} \quad \frac{L}{R} + K_{us}\alpha_y \tag{3.32}$$

From (3.32), the understeer gradient is labeled as K_{US} and is defined as:

$$K_{US} = \frac{1}{g} \quad \frac{W_f}{C_{\alpha f}} \quad \frac{W_r}{C_{\alpha r}} \div \tag{3.33}$$

$$K_{US} = \frac{m}{L} \quad \frac{bC_{\alpha r} \quad aC_{\alpha f}}{C_{\alpha r}C_{\alpha f}} \div$$

The understeer gradient determines both the magnitude and the direction of the steering inputs required for a given lateral acceleration [16]. The understeer gradient also determines if the vehicle is neutral steer, oversteer, or understeer. Figure 3.7 shows the basic principles with K_{US} being the slope of each line.

3.3.2.1 Neutral Steer

Neutral steer occurs when the understeer gradient is zero, which results in the front and rear steady-state tire slip angles being equivalent. By studying (3.16), during neutral steer the steer angle required to make the turn is approximately the Ackerman angle.

3.3.2.2 Understeer

Understeer occurs when K_{US} is greater than zero, causing larger slip angles to develop in the front tire than the rear. Because there is more slip at the front tire, the steer angle must increase to maintain the radius of the curve. During this condition, the steer angle increases linearly with the speed squared or the lateral acceleration.

3.3.2.3 Oversteer

Oversteer is the opposite of understeer. During oversteer, K_{US} is less than zero causing the rear tire slip angle to be greater than the front. Because the rear is sliding more than the front, less steer angle is required to navigate the turn.

3.3.3 Four-Wheel Bicycle Model

To cope with the effects of roll, roll models are used. This often requires modifying the bicycle model into a four-wheel bicycle model. The four-wheel

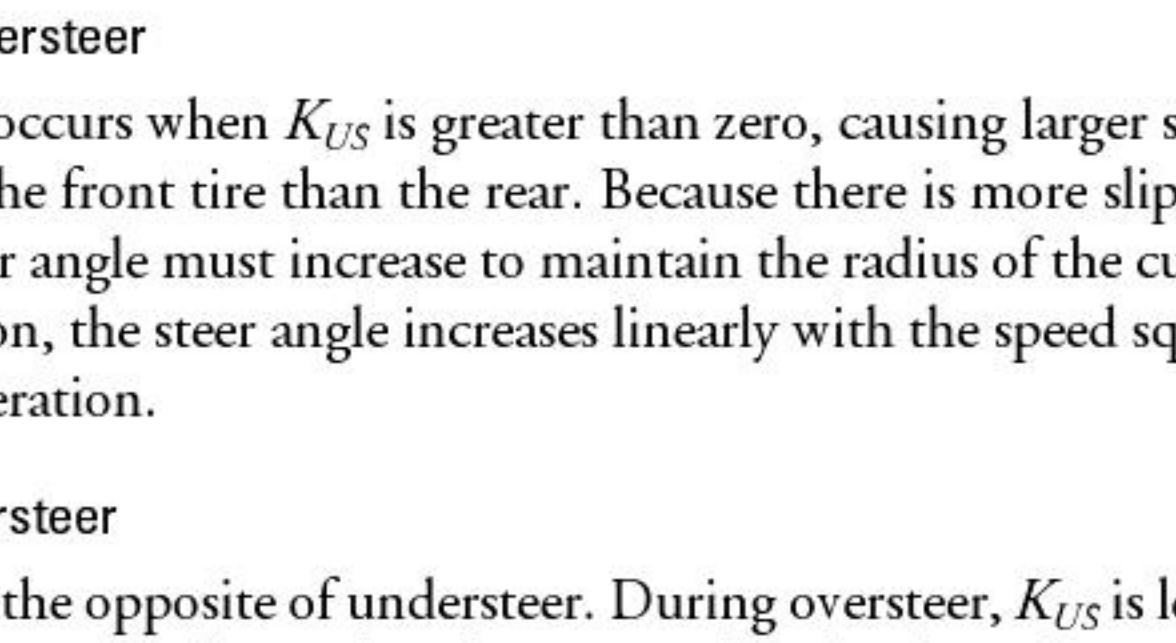

Figure 3.7 Basic understeer gradient plot.

bicycle model accounts for the difference between the inner and outer vertical tire forces. This difference is the weight transfer. Weight transfer is important to understand because the vertical force on tire affects the lateral and longitudinal forces of the tire that dictate the performance of handling dynamics and characteristics. Before exploring roll models, tire models and properties will be discussed.

The dynamic equations of motion for a ground vehicle model are derived for a vehicle that possesses both front and rear steering capabilities as well as individual torque control of each wheel. This general model is easily adapted to simpler vehicles (e.g., vehicles with only front-wheel steering), by the assignment of a constant control input of zero to the appropriate (unavailable) control effectors. The free body diagram for the vehicle under consideration is shown in Figure 3.8. A right-handed coordinate system is used for the derivation of the equations of motion. The body fixed reference frame has an origin at the vehicle's center of gravity. The z-axis is pointing down toward the ground, the x-axis is pointing toward the front of the vehicle, and the y-axis is pointing out to the vehicle's passenger side. In Figure 3.8, r is the yaw rate, $V = [\dot{x}\,\dot{y}]^T$ is the velocity vector acting at the vehicle's center of gravity, β represents sideslip angle, δ is the steering angle, t is the track width, and a and b are distances from the vehicle center of gravity to the front and rear axles,

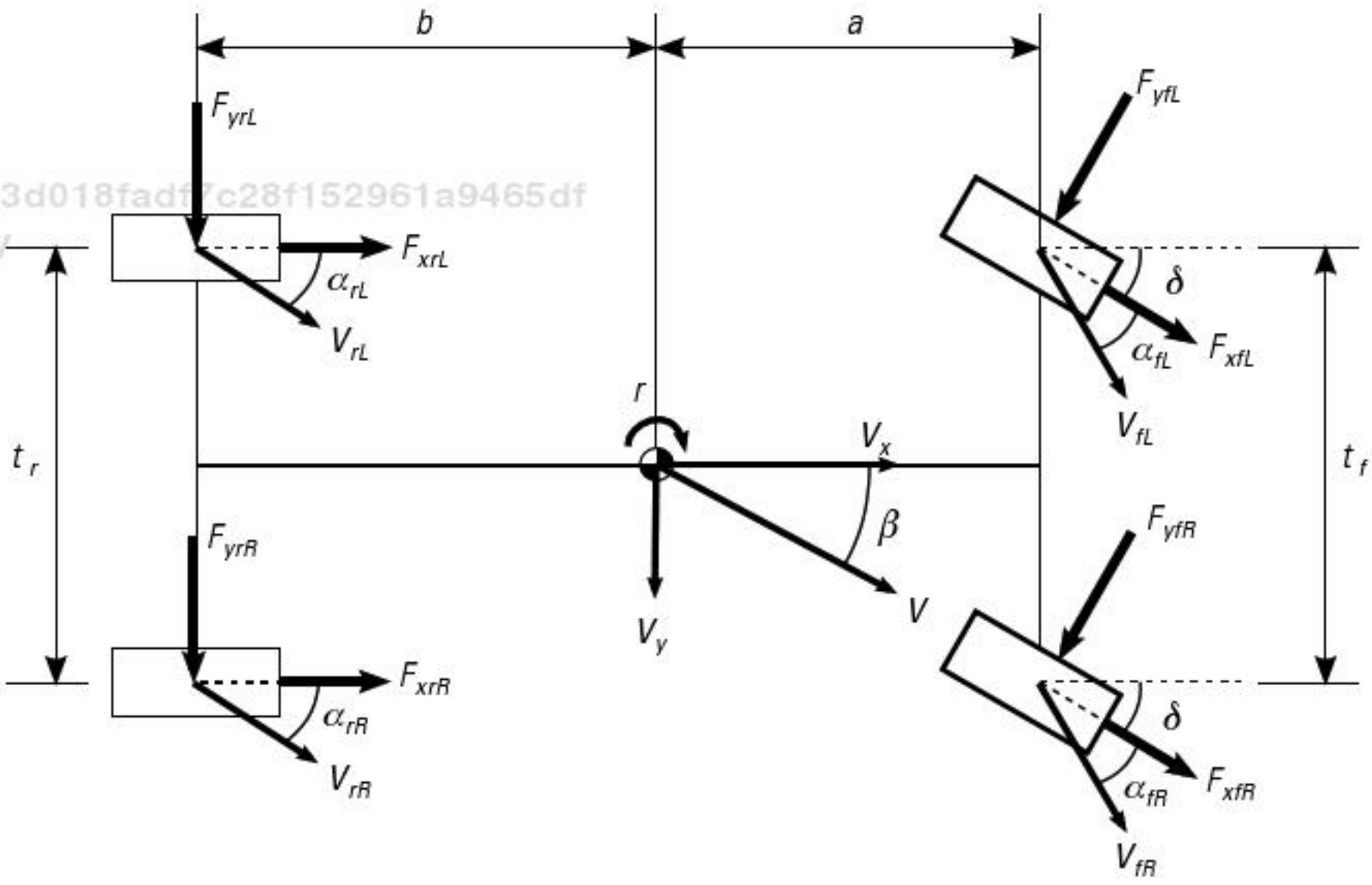

Figure 3.8 Four-wheel bicycle model.

respectively. Subscripts *f*, *r*, *R*, *L* denote front, rear, right, and left sides of the vehicle, respectively. For clarity, only the left slip angles (α_{fL} and α_{rL}) and the right steer angles (δ_{fR} and δ_{fL}) are shown on Figure 3.8. This model assumes that left and right steer angles are the same for front and rear axles. Note that all forces F and slip angles α are drawn in the positive direction such that the lateral force $F =\quad C_\alpha\alpha$ where C_α represents tire cornering stiffness.

The sum of the moments about the vehicle's center of gravity is written as

$$\begin{aligned} M_{cg} = I_z\ddot{\psi} = a(&F_{yfL}\cos\delta_f + F_{yfR}\cos\delta_f \quad F_{xfL}\sin\delta_f \quad F_{xfR}\sin\delta_f) \\ &\frac{t_f}{2}(F_{ylF}\sin\delta_f \quad F_{yfR}\sin\delta_f \quad F_{xfL}\cos\delta_f + F_{xfR}\cos\delta_f) \\ &b\,(F_{yrL}\cos\delta_r + F_{yrR}\cos\delta_r + F_{xrL}\sin\delta_r + F_{xrR}\sin\delta_r) \\ &\frac{t_r}{2}(F_{yrL}\sin\delta_r \quad F_{yrR}\sin\delta_r \quad F_{xrL}\cos\delta_r + F_{xrR}\cos\delta_r) \end{aligned} \tag{3.34}$$

where I_z is the moment of inertia about the yaw axis. The solution of (3.34) for $\ddot{\psi}$ yields

$$\begin{aligned} \ddot{\psi} = \dot{r} = \; & a\left((F_{yfL} + F_{yfR})\cos\delta_f \quad (F_{xfL} + F_{xfR})\sin\delta_f\right) \\ & \frac{t_f}{2}\left((F_{ylF} + F_{yfR})\sin\delta_f \quad (F_{xfL} \quad F_{xfR})\cos\delta_f\right) \\ & b\left((F_{yrL} + F_{yrR})\cos\delta_r + (F_{xrL} + F_{xrR})\sin\delta_r\right) \\ & \frac{t_r}{2}\left((F_{yrL} \quad F_{yrR})\sin\delta_r \quad (F_{xrL} \quad F_{xrR})\cos\delta_r\right) / I_z \end{aligned} \tag{3.35}$$

which describes the nonlinear yaw dynamics of the vehicle.

The sideslip angle β is the angle between the vehicle's actual velocity vector V and its longitudinal velocity component V_x. Therefore, the vehicle fixed velocities and corresponding accelerations due to sideslip are

$$\begin{aligned} V_x &= V\cos\beta \quad \dot{V}_x = \dot{V}\cos\beta \quad V\dot{\beta}\sin\beta \\ V_y &= V\sin\beta \quad \dot{V}_y = \dot{V}\sin\beta + V\dot{\beta}\cos\beta \end{aligned} \tag{3.36}$$

The effects of yaw rate are then included to give the complete expressions for acceleration in the vehicle fixed reference frame

$$\ddot{x} = \dot{V}\cos\beta \quad V\dot{\beta}\sin\beta \quad rV\sin\beta \tag{3.37}$$

$$\ddot{y} = \dot{V}\sin\beta \quad V\dot{\beta}\cos\beta \quad rV\cos\beta \tag{3.38}$$

The summation of the forces in the y-axis yields

$$F_y = m\ddot{y} = (F_{yfL} + F_{yfR})\cos\delta_f + (F_{xfL} + F_{xfR})\sin\delta_f + (F_{yrL} + F_{yrR})\cos\delta_r + (F_{xrL} + F_{xrR})\sin\delta_r \tag{3.39}$$

Equation (3.38) is substituted into (3.39) and solved for $\dot{\beta}$ to obtain the equation of motion for sideslip

$$\dot{\beta} = \left[(F_{yfL} + F_{yfR})\cos\delta_f + (F_{xfL} + F_{xfR})\sin\delta_f + (F_{yrL} + F_{yrR})\cos\delta_r + (F_{xrL} + F_{xrR})\sin\delta_r\right] / (mV\cos\beta) \quad \dot{V}\tan\beta/V \quad r \tag{3.40}$$

3.4 Tires

3.4.1 Basics

The tire-road relationship is governed by the contact patch. With the exception of aerodynamic forces, all external forces on the vehicle are developed at the tire's contact patch. The tire serves three basic functions:

1. It supports the vertical load, while cushioning against road shocks.
2. It develops longitudinal forces for acceleration and braking.
3. It develops lateral forces for cornering.

3.4.2 Contact Patch and Slip

Due to the elastic properties of the tire the contact patch deforms under loads. This deformation results in the slip angle α. Experimental data shows

that the lateral force on a tire displays a nonlinear relationship with the slip angle "alpha." However, there is a linear portion for small angles of α. The slope of this linear portion is called the cornering stiffness C_α. Equations (3.10) and (3.11) can be derived from the linear portion of experimental data similar to the data shown in Figure 3.9.

Figure 3.9 shows typical characteristics of a tire under lateral force generation modeled by the Fiala tire model. More information on this model will be discussed later. As shown in the plot, the lateral tire force remains linear with slip angle, as modeled by (3.10) and (3.11), until the tire becomes saturated. This model relates peak tire force to the tire-road friction, μ, times the normal force, F_z, known as the peak tire force.

An increase in the normal or vertical force of a tire will cause the relationship between the lateral force and the slip angle to change. This increase will yield a higher peak tire force. Vertical forces on the tire are not only important for ride characteristics, but also help to describe the maximum longitudinal and lateral forces developed by the tire. As shown in Figure 3.10, the magnitude of lateral and longitudinal tire force cannot exceed the peak tire force. When the magnitude of tire force reaches this point, sliding occurs. By studying Figure 3.10, it is obvious that the available longitudinal

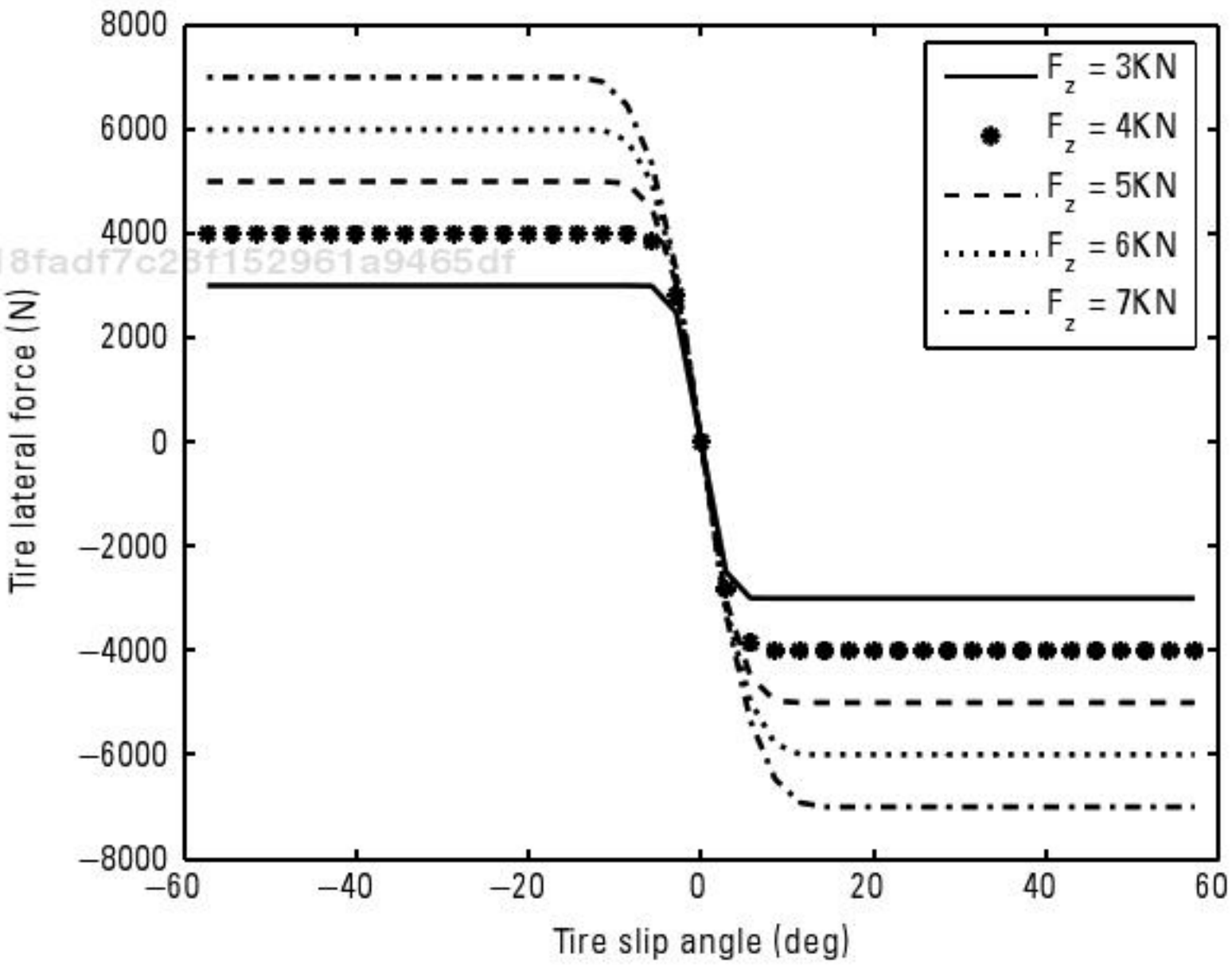

Figure 3.9 Generic tire curve.

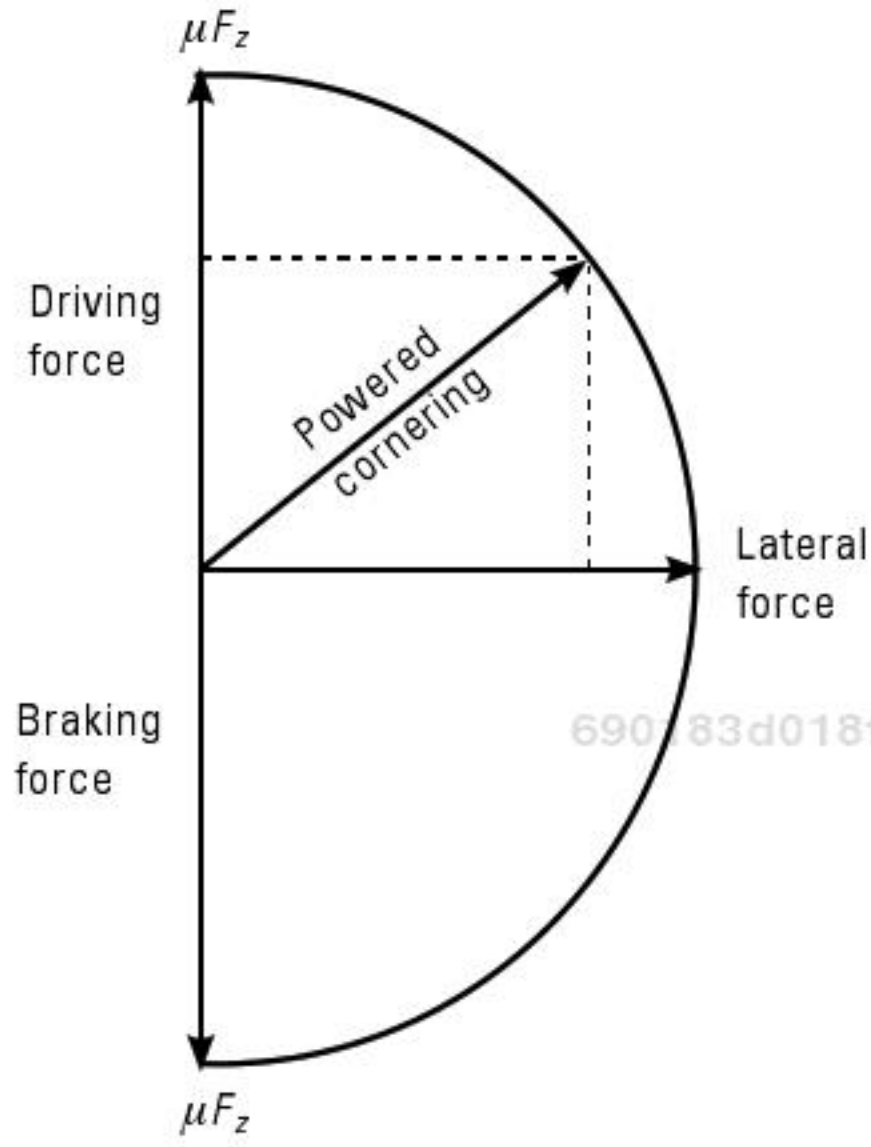

Figure 3.10 Circle of friction for tire forces.

drive and braking force decreases with an increase in lateral force. Because of this effect, both forces must be taken into account during combined lateral and longitudinal tire force generation to develop an accurate vehicle model.

3.4.3 Tire Models

Several researchers have developed models to describe the generated tire forces. One of the most well-known models, called the Magic Formula tire model, was developed by Pacejka [4, 5, 7]. This model is an empirical formula capable of calculating lateral and longitudinal tire forces. Alternatively, the two models used in this book are the Fiala and Dugoff tire model.

3.4.3.1 Fiala Tire Model

The Fiala tire model was originally developed to estimate lateral tire force generation only [2]. The model, however, was transformed to represent both lateral and longitudinal forces [3]. To accomplish this transformation lateral and longitudinal tire stiffness (C_α, C_σ) are assumed to be equal. This assumption though does not always hold true. The total slip σ for this model

is simply the magnitude of the lateral and longitudinal slip (σ_y, σ_x), shown by (3.41).

$$\sigma = \sqrt{\sigma_y^2 + \sigma_x^2} \tag{3.41}$$

To calculate the total slip, the individual values for slip must be known. Both the longitudinal and lateral slips are found using (3.42) and (3.43).

$$\sigma_x = \frac{r_{eff}\omega_w \quad V_x}{r_{eff}\omega_w} \; during\ acceleration$$

$$\sigma_x = \frac{V_x}{r_{eff}\omega_w} \; during\ braking \tag{3.42}$$

$$\sigma_y = \frac{V_x}{r_{eff}\omega_w}\tan(\alpha) \tag{3.43}$$

Both slip values can be determined with the use of sensors. Assuming a parabolic pressure distribution on the tire's contact patch, (3.44) is used to describe the magnitude of force on the tire, using the Fiala tire model.

$$\mu F_z \quad 3\theta\sigma \quad \frac{1}{3}(3\theta\sigma)^2 + \frac{1}{27}(3\theta\sigma)^3 \quad if\ \sigma \quad \sigma_m$$

$$F = \mu F_z \; if\ \sigma \quad \sigma_m \tag{3.44}$$

The variable, σ_m, is the value of total slip where sliding occurs in the Fiala tire model. As described by the circle of friction, sliding is assumed to begin when the maximum tire force is equal to μF_z.

$$\sigma_m = \frac{1}{\theta} = \frac{3\mu F_z}{C_{\alpha/\sigma}} \tag{3.45}$$

The individual values of lateral and longitudinal tire force (F_y, F_x) can be obtained by breaking up the force magnitude F_t. This is done by multiplying the force magnitude by the ratio of total slip to each forces respective slip, as shown in (3.46) and (3.47).

$$F_x = \frac{\sigma_x}{\sigma}F \tag{3.46}$$

$$F_y = \frac{\sigma_x}{\sigma} F \tag{3.47}$$

In the case of pure lateral slip, set $\sigma_y = \tan(\alpha)$ and $\sigma_x = 0$ in the Fiala tire model. In case of pure longitudinal slip, set $\sigma_y = 0$ [10]. By reducing the combined force generation model to either lateral or longitudinal force generation, simpler calculations can be performed if the amount of noisy measurements is reduced.

3.4.3.2 Dugoff Tire Model

The Dugoff model and Fiala model both allow for tire force estimates during combined lateral and longitudinal tire force generation. However, the Dugoff tire model assumes a uniform vertical pressure distribution on the tire's contact patch [6]. This is a simplification from the Fiala's tire model, but it allows for individual values of lateral and longitudinal tire stiffness. The longitudinal and lateral tire forces are given by (3.48) and (3.49), respectively.

$$F_x = C_\alpha \frac{\sigma_x}{1+\sigma_x} f(\lambda) \tag{3.48}$$

$$F_y = \frac{C_\alpha \tan(\alpha)}{1+\sigma_x} f(\lambda) \tag{3.49}$$

where

$$\lambda = \frac{uF_z(1+\sigma_x)}{2\ (C_\sigma \sigma_x)^2 + (C_\alpha \tan(\alpha))^2\ ^{\frac{1}{2}}} \tag{3.50}$$

$$f(\lambda) = \begin{matrix} (2 \quad \lambda)\lambda & if\ \lambda < 1 \\ 1 & if\ \lambda \quad 1 \end{matrix} \tag{3.51}$$

Similar to the Fiala tire model, this model has a transition that occurs when $\lambda = 1$. This transition occurs when the tire leaves the linear region and begins the nonlinear region. If the tire is experiencing lateral slip only, the model may be reduced by setting $\sigma_x = 0$ or for pure longitudinal force generation simply set $\alpha = 0$. This helps to simplify the model during driving conditions where only lateral or longitudinal forces are generated.

3.5 Roll Model

It is very important to understand vehicle roll and rollover. Many researchers have developed models to describe the roll dynamics of vehicles during cornering. Some models are fairly simple while others are very in depth and require more parameters. The less complex roll models do not include the springs and dampers of the suspension and therefore assume the sprung mass is stationary with the axle. Other high-fidelity models take into account forces produced by the springs and dampers.

3.5.1 Free Body Diagram

In order to produce a reliable roll model, a free body diagram (FBD) must be developed. The FBD in Figure 3.11 shows a two-state roll plane model [13, 14]. Three important parameters used in this model include the CG height, h_{cg}, roll stiffness, K_ϕ, and roll damping coefficient, C_ϕ. This model lumps the entire vehicle mass into the sprung mass. This assumption allows a simplified equation for the spring and damper torques, shown in (3.52) and (3.53).

$$T_{spring} = K_\phi \phi \tag{3.52}$$

$$T_{damper} = C_\phi \dot{\phi} \tag{3.53}$$

Notice that both equations also assume the spring and damper torques are linear with roll, ϕ, and roll rate, $\dot{\phi}$, respectively. Also, note that $\dot{\phi}$ is equivalent to p, the SAE defined roll rate.

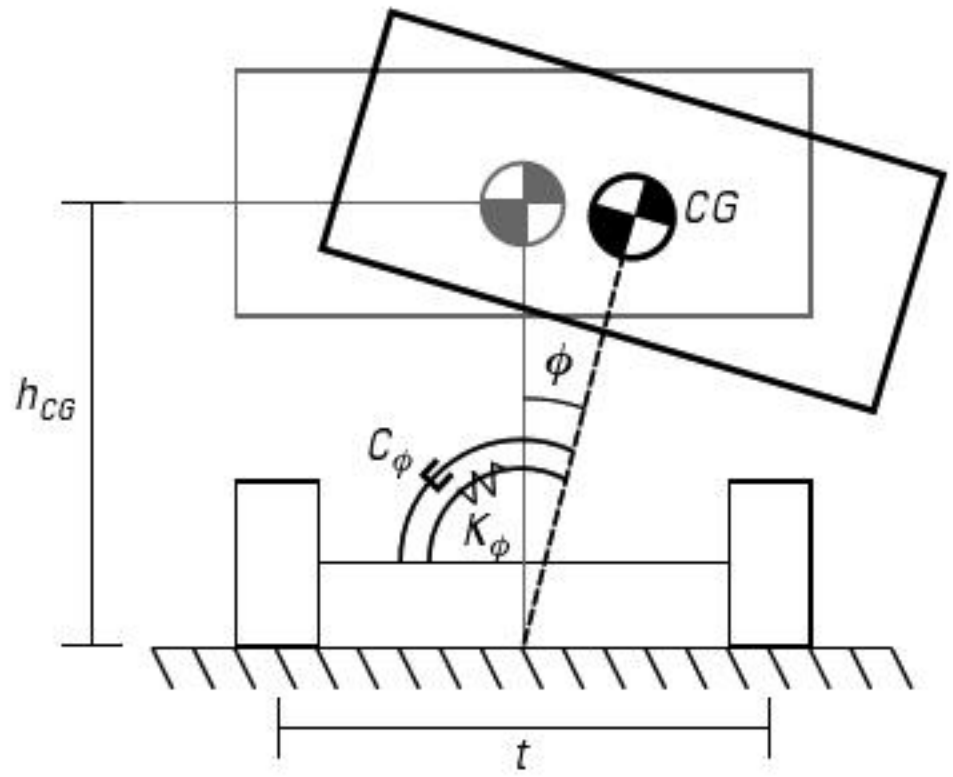

Figure 3.11 Vehicle roll free body diagram.

3.5.2 Equation of Motion

By summing the moments about the roll center on Figure 3.11, a simple equation is derived to describe the roll dynamics of the vehicle. Equation (3.54) assumes the vehicle's sprung mass rotates about a fixed point at the centerline of the lateral axis on the ground.

$$J_{eff}\ddot{\phi} + C_{\phi}\dot{\phi} + K_{\phi}\phi = mh_{cg}(a_y\cos(\phi) + g\sin(\phi)) \tag{3.54}$$

By assuming a steady-state turn and small angles, (3.54) can be simplified to solve for the roll angle with knowledge of the CG height and the spring roll stiffness.

$$\phi = \frac{mh_{cg}a_y}{K_{\phi} \quad mh_{cg}g} = \frac{mh_{cg}V^2}{R(K_{\phi} \quad mh_{cg}g)} \tag{3.55}$$

3.5.3 State Space Representation

Equation (3.55) may be transformed into a state space representation. The state space representation is shown in (3.56).

$$\begin{matrix}\dot{\phi}\\ \ddot{\phi}\end{matrix} = \begin{matrix}0\\ \frac{K_{\phi} \quad mgh_{cg}}{J_{eff}}\end{matrix} \quad \begin{matrix}1\\ \frac{C_{\phi}}{J_{eff}}\end{matrix} \quad \begin{matrix}\phi\\ \dot{\phi}\end{matrix} + \begin{matrix}0\\ \frac{mh_{cg}}{J_{eff}}\end{matrix} a_y \tag{3.56}$$

Many other models have also been used to analyze roll dynamics. Some models developed do not assume the vehicle's roll center is located at ground height. One model developed in [11, 12] assumes the roll center is not at ground level and that the imaginary roll center derived produces reactionary forces.

3.6 Additional Models Used in this Work

In addition to the bicycle models two other models are used in later chapters to describe two-wheeled vehicles and trailer dynamics.

3.6.1 Two-Wheeled Vehicle

The two-wheeled vehicle motion is modeled as a kinematic relationship to describe the position changes as shown in Figure 3.12.

The variable $\theta = [\theta_L, \theta_R]$ represents angular positions of the robot wheels. The variable d is the distance between the driving wheels, or track width. The vehicle's change in position in the East, North, Up (ENU) Cartesian coordinate frame can be found from the following kinematic equations.

$$\dot{\psi} = r \tag{3.57}$$

$$\dot{e} = V_x \sin\psi \tag{3.58}$$

$$\dot{n} = V_x \cos\psi \tag{3.59}$$

where

$$V_x = \frac{R}{2}(\dot{\theta}_R + \dot{\theta}_L) \tag{3.60}$$

$$r = \frac{R}{d}(\dot{\theta}_L \quad \dot{\theta}_R) \tag{3.61}$$

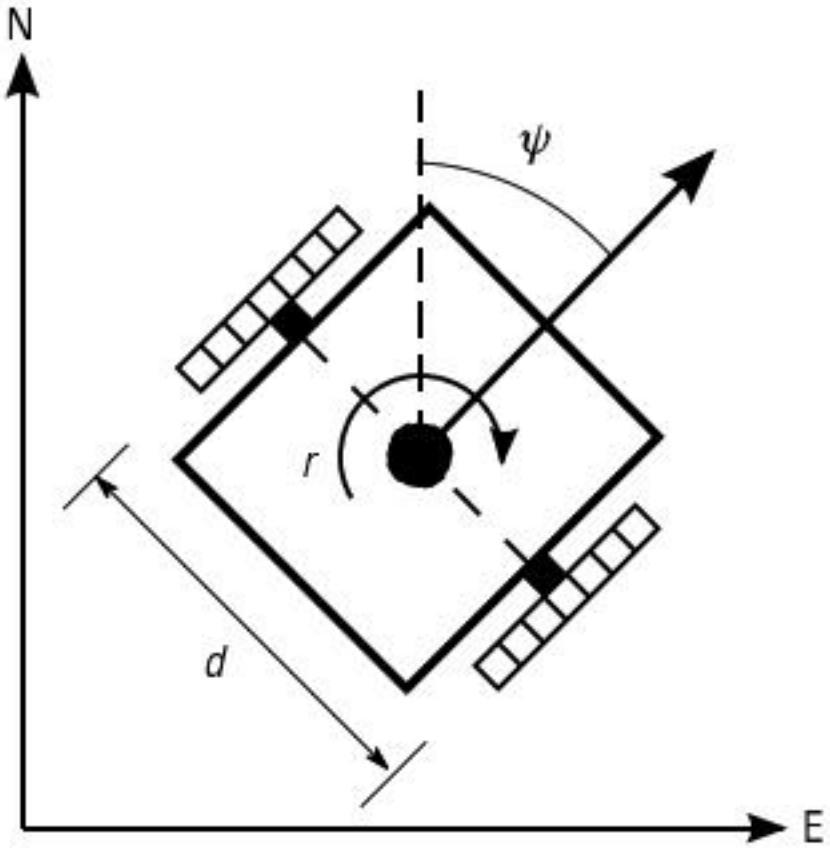

Figure 3.12 Two-wheeled vehicle kinematic diagram.

A state space representation of the transform from body fixed XYZ frame to the global ENU frame is shown in (3.62).

$$\begin{matrix} \dot{e} \\ \dot{n} \\ \dot{\psi} \end{matrix} = \begin{matrix} \sin\psi \\ \cos\psi \\ 0 \end{matrix} V_x + \begin{matrix} 0 \\ 0 \\ 1 \end{matrix} r \tag{3.62}$$

3.6.2 Trailer Model

A kinematic model is used to describe a trailer or implement towed behind the vehicle. A schematic of a vehicle pulling a trailer is shown in Figure 3.13. The trailer's point of zero lateral velocity, ZLV, as well as its control point,

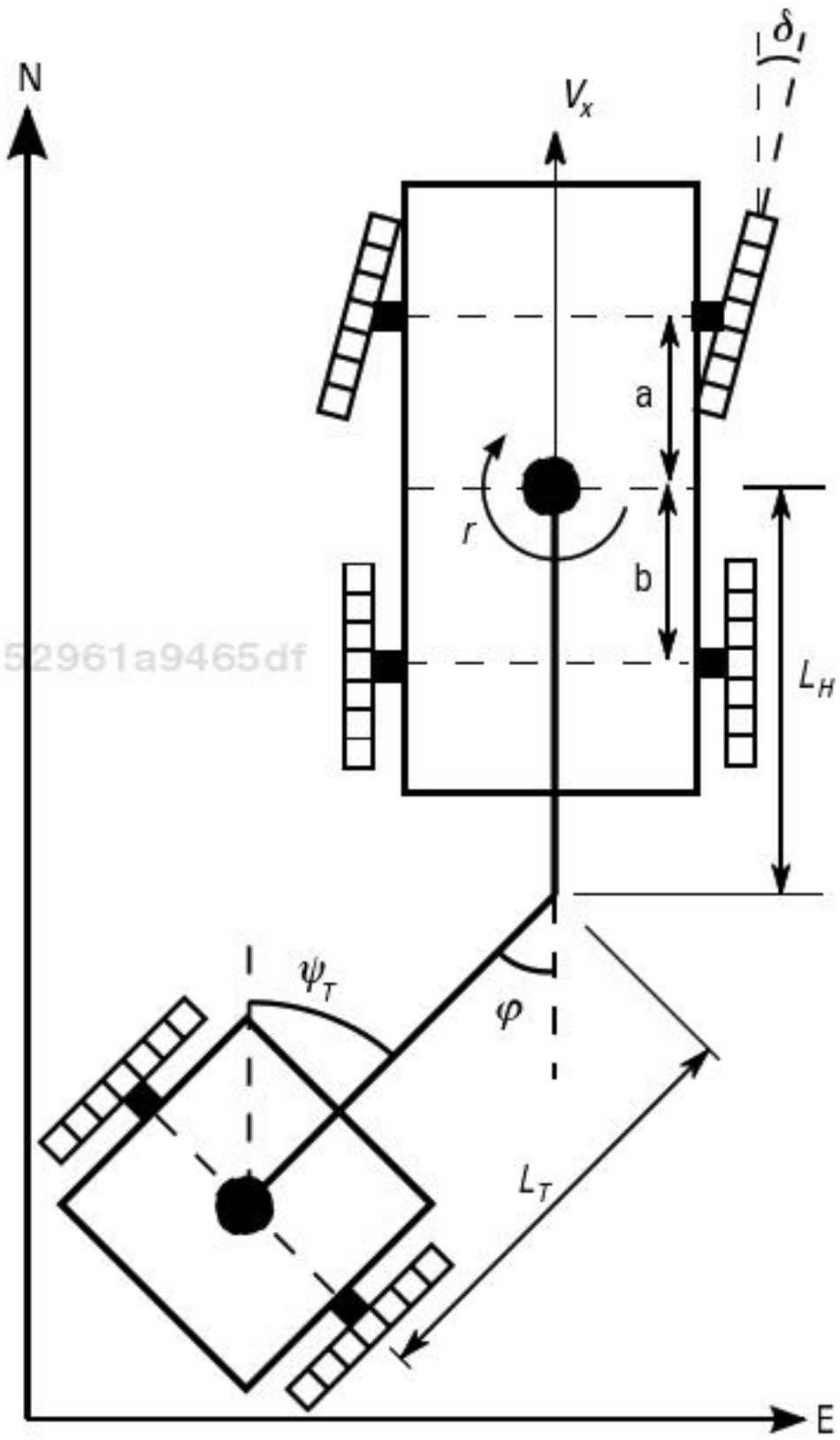

Figure 3.13 Vehicle-trailer free body diagram.

cp, are shown in Figure 3.13. The ZLV is the point on the implement where the lateral velocity is equal to zero. For a two-wheeled trailer, the ZLV point is assumed to be the point at the center of the axle between the two wheels. For farm implements or more complicated trailer designs, more sophisticated system identification techniques may be required to determine the ZLV point. The control point defines the point on the trailer that should follow the specified path. This point can be chosen by the designer and is often chosen to be the location of the GPS antenna on the trailer if one is used to determine the trailer's position.

A kinematic model that relates the vehicle velocity, V_x, and yaw rate, r, to the angle between the vehicle and the trailer is referred to as the hitch angle, φ, and is given by (3.63)

$$\dot{\varphi} = r\left(1+\frac{L_H}{L_T}\cos\varphi\right) \div \frac{V_x}{L_T}\sin\varphi \tag{3.63}$$

where L_H is the distance from the CG of the vehicle to the hitch point and L_T is the distance from the hitch point to the ZLV point of the trailer. The model is derived by looking at how vehicle velocity and yaw rate translate into velocities at the tow pin. The resulting tow pin velocities can then be used to determine the rotational velocity of the implement assuming zero lateral velocity at the ZLV point.

Table 3.1
Properties of Carsim's G35 Sedan

Wheelbase	L	2.85m
Vehicle Mass	m	940 kg
Dist. from CG to Front Contact Patch	a	1.019m
Dist. from CG to Rear Contact Patch	b	1.831m
Yaw Moment of Inertia	I_z	1,530 kg * m^2
Front Tire Cornering Stiffness	$C_{\alpha f}$	78,311 N/rad
Rear Tire Cornering Stiffness	$C_{\alpha r}$	47,033 N/rad
Injected Noise Value on a_y	$\sigma^2_{\alpha_y}$	$(.1\ m/s^2)^2$
Injected Noise Value on r	σ^2_r	$(.02\ rad/s)^2$
Injected Noise Value on β	σ^2_β	$(.02\ rad)^2$
Injected Noise Value on V	σ^2_v	$(.01\ m/s)^2$

3.7 Vehicle Model Validation

To show the accuracy and limitations of the models, each model is validated with experimental data. The data is from a G35 sedan at the National Center for Asphalt Technology (NCAT) test track. The Infiniti G35 sedan is implemented with a dual antenna GPS unit, wheel speed sensor, a 6 DOF inertial measurement unit (IMU), and an optical encoder for steer angle measurements. Carsim, a high-fidelity vehicle simulation software, is also used for roll model verification.

With the data gathered at the NCAT test track, the kinematic and bicycle model are validated in MATLAB. The parameter values used in the simulations of the G35 sedan are listed in Table 3.1.

By using MATLAB to simulate the dynamic equations presented in this chapter, Figure 3.14 shows that both the kinematic and bicycle model matches the recorded data at 2 m/s, as would be expected. However, for larger slip angles, the assumptions of the kinematic model break down causing the

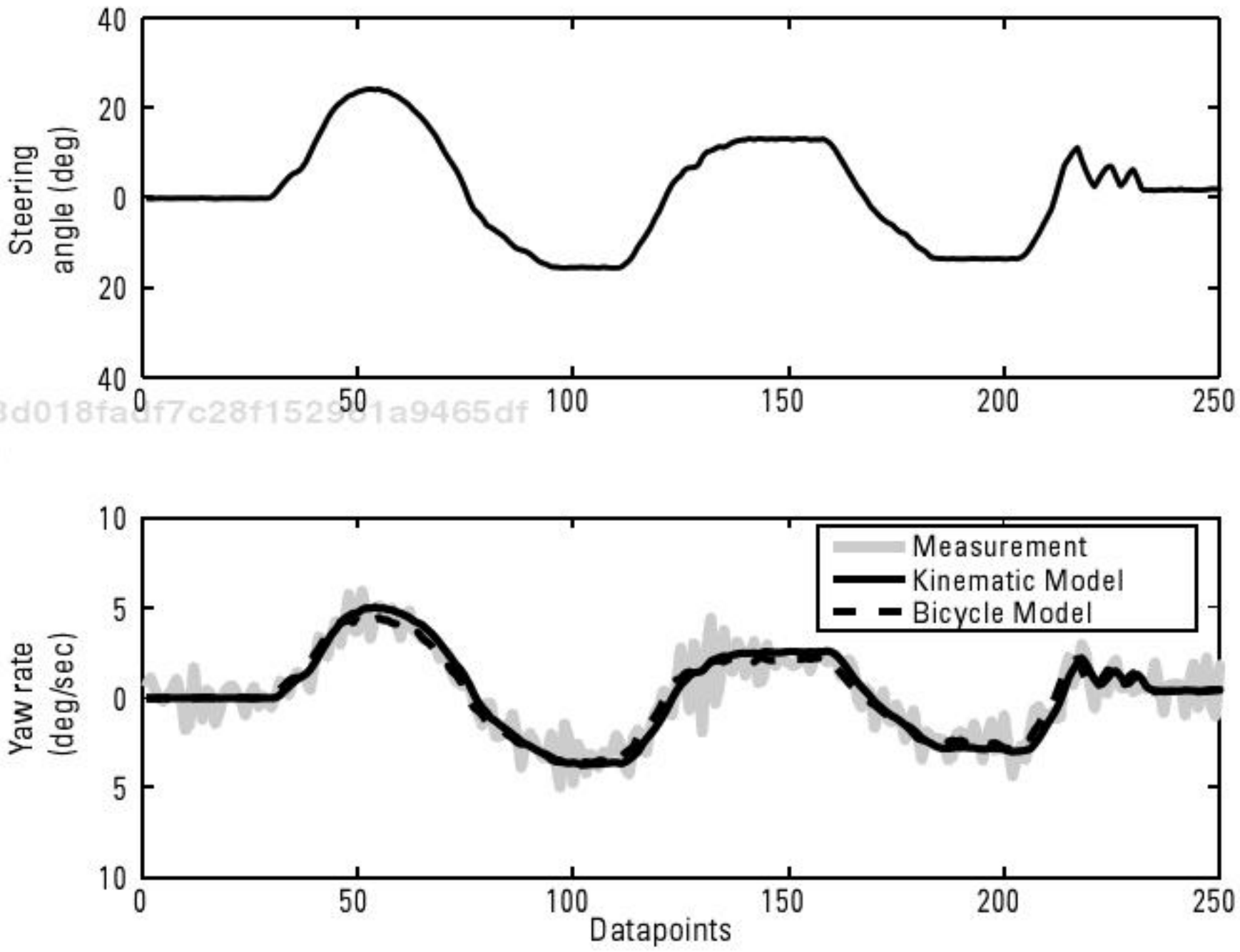

Figure 3.14 Comparison of the kinematic and bicycle model during slow-speed turning in the G35 sedan.

model to perform poorly. In the data logged at NCAT, slip angles remained small enough for both the bicycle and kinematic model to hold true. When vehicles reach higher speeds, as shown in the next experiment, the simplistic kinematic model is not the best choice.

To show the shortcomings of the kinematic model, data was logged in a G35 sedan at higher speeds around the NCAT test track. The inputs were run through both models in MATLAB and the results are shown in Figure 3.15. Notice the difference in the kinematic and bicycle models prediction of yaw rate. While cornering at high speeds with large slip angles, the kinematic model cannot accurately predict the vehicle's dynamics.

To illustrate the shortcomings of the bicycle model with a linear tire model, a maneuver is conducted that saturates the tires enough for the vehicle to begin sliding. This is a very hard maneuver and is conducted to show that

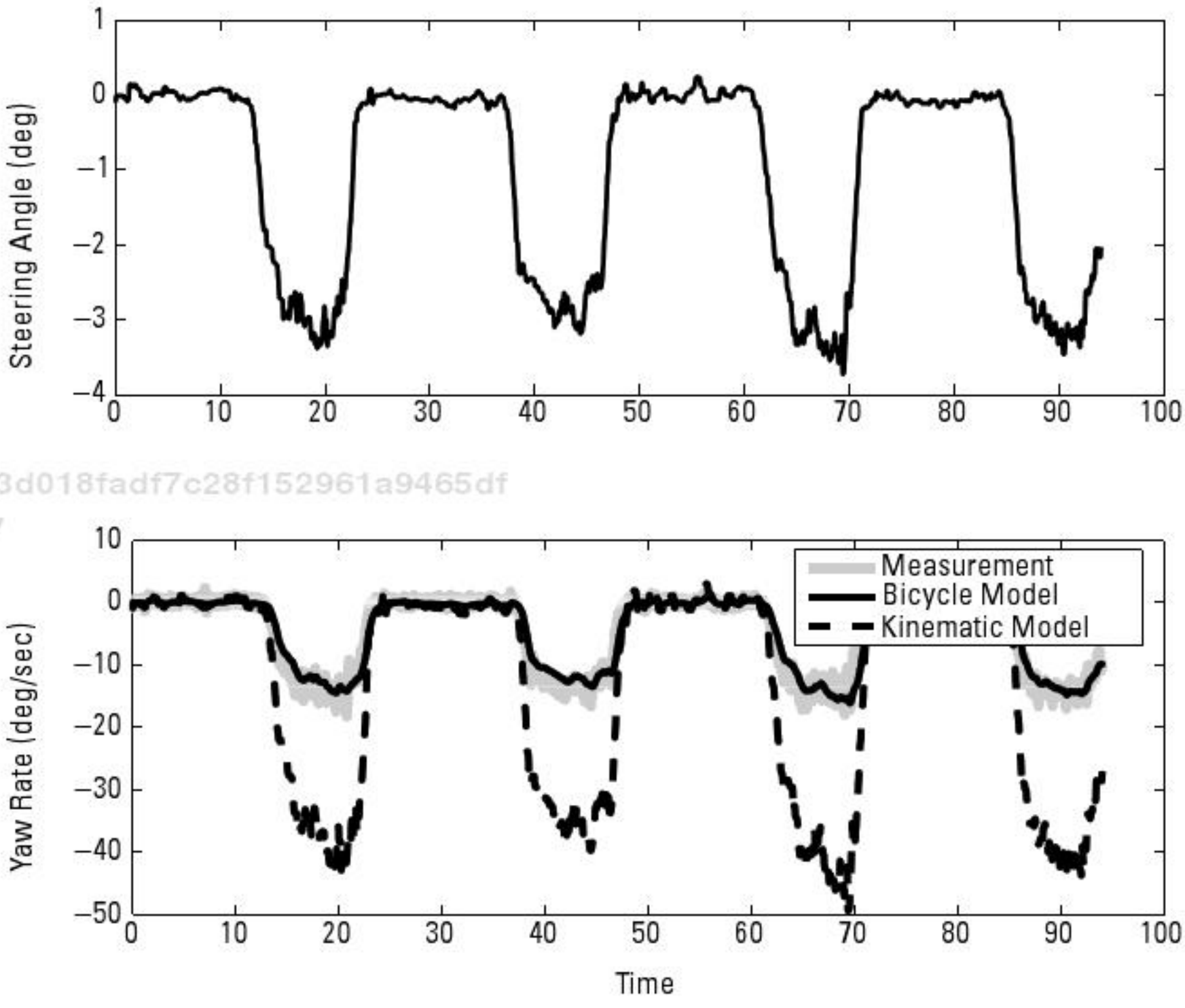

Figure 3.15 Comparison of the kinematic and bicycle model during high-speed cornering in the G35 sedan.

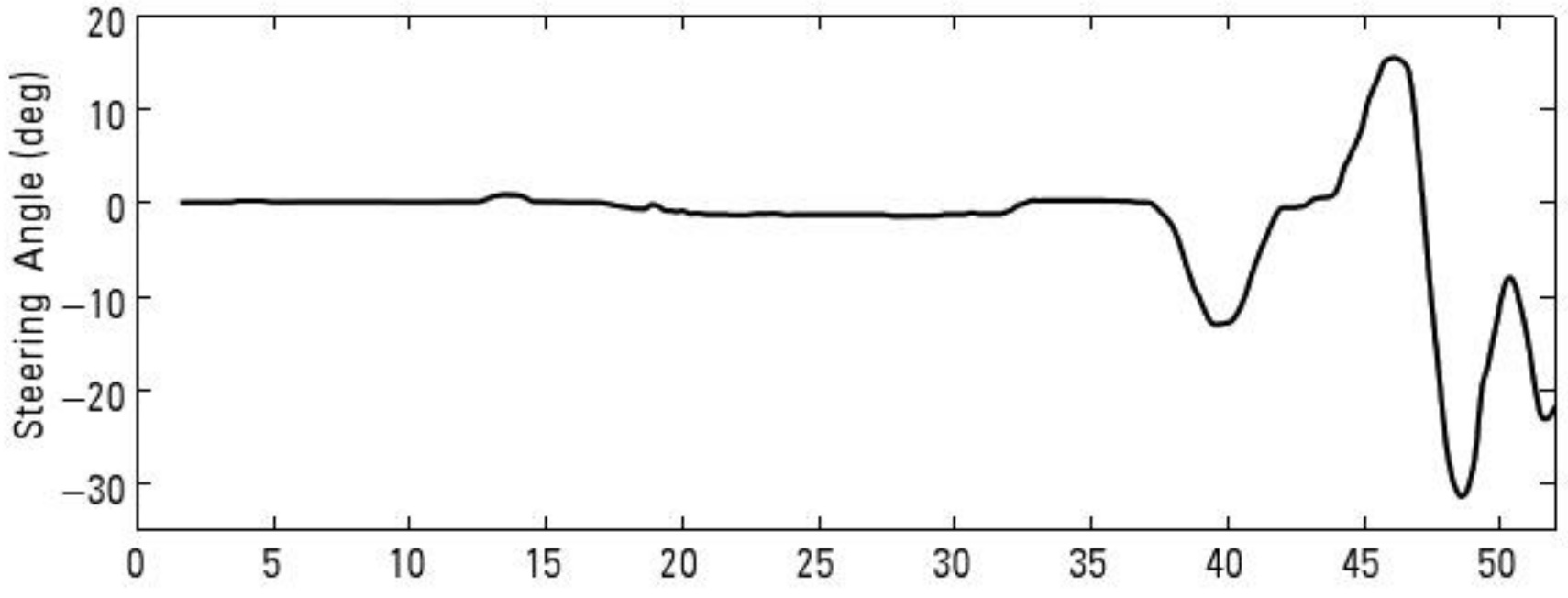

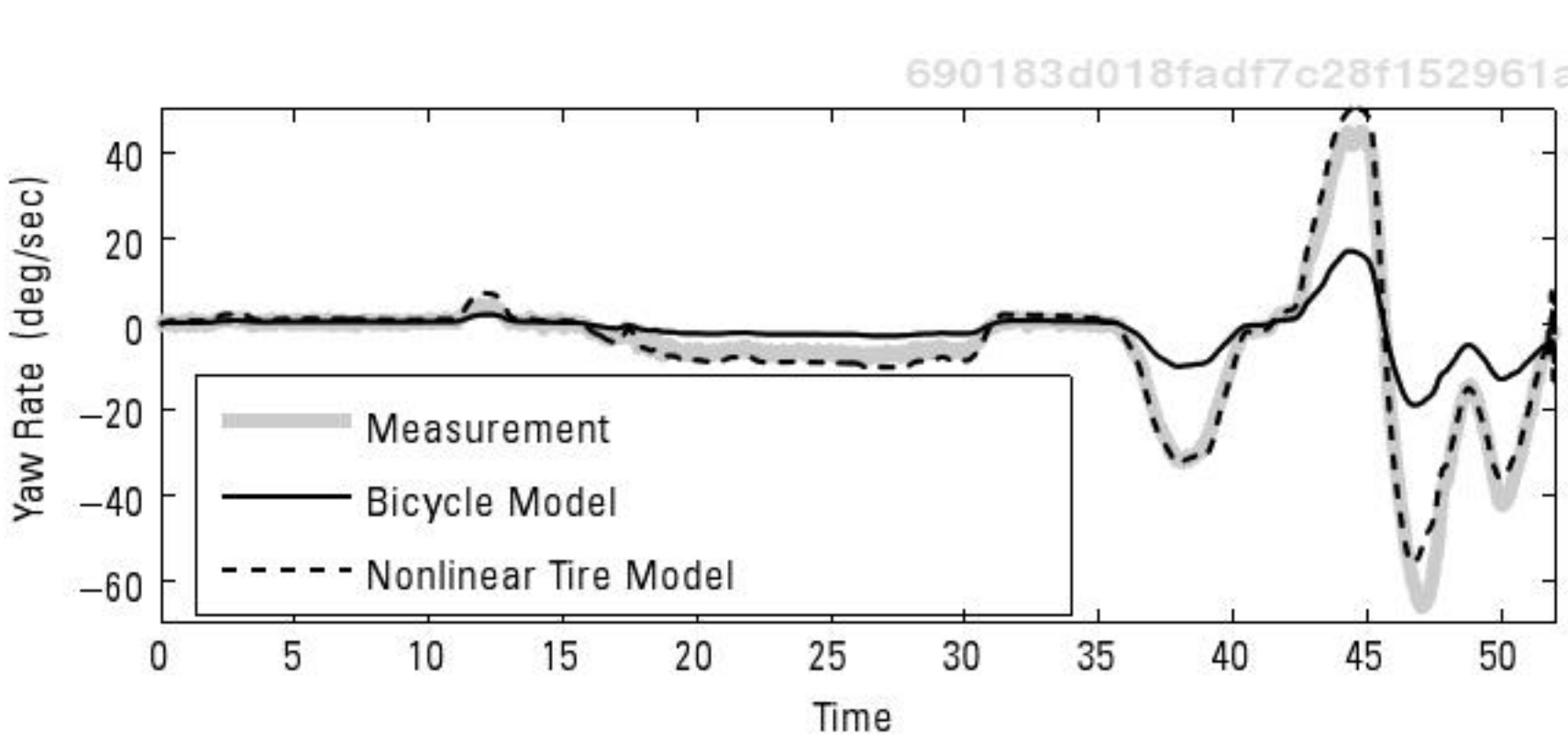

Figure 3.16 Comparison of the bicycle model with linear and nonlinear tire models during high-speed sliding experiments in the G35 sedan.

a linear tire model without saturation cannot describe the vehicle motion at the limits of handling. The more advanced model uses the Dugoff tire model to calculate the lateral tire forces. Figure 3.16 shows the bicycle model with a linear tire failing to match the data when the vehicle loses control. However, the bicycle model with a nonlinear tire model matches the data fairly well, although there is still some mismatch at the highest peak. This is most likely due to the fact that the model does not take into account vehicle roll dynamics.

Finally, the two-state roll plane model is tested. The vehicle used in this simulation is a large SUV from Carsim. Carsim is a high-fidelity vehicle simulation tool that can be used to validate simplified vehicle models. Carsim is chosen in this experiment because a vehicle is needed that produces large roll angles, unlike the G35 sedan used in previous experiments. Table 3.2 provides the parameter values used in the roll plane model during this simulation.

Table 3.2
Properties of Carsim's Large SUV

Vehicle Mass	m	2,450 kg
CG Height (Sprung Mass)	h_{CG}	1.1m
Roll Mass Moment of Inertia	J_{eff}	1,243 kg * m^2
Roll Stiffness	K_ϕ	2,527.9 $\frac{N \quad m}{deg}$
Roll Damping	C_ϕ	152.05 $\frac{N \quad m \quad s}{deg}$
Track Width	T	1.62m
Injected Noise Value on a_y	$\sigma^2_{a_y}$	$(.1\ m/s^2)^2$
Injected Noise Value on ϕ	σ^2_{ϕ}	$(.01\ rad)^2$
Injected Noise Value on $\dot{\phi}$	$\sigma^2_{\dot{\phi}}$	$(.005\ rad/s)^2$

The large SUV attempts a double-lane change in order to induce large roll rates and angles. The data from Carsim is used to compare with the simple two-state roll plane model, which is simulated in MATLAB. The data from Carsim matches up well with the simple roll plane model, given

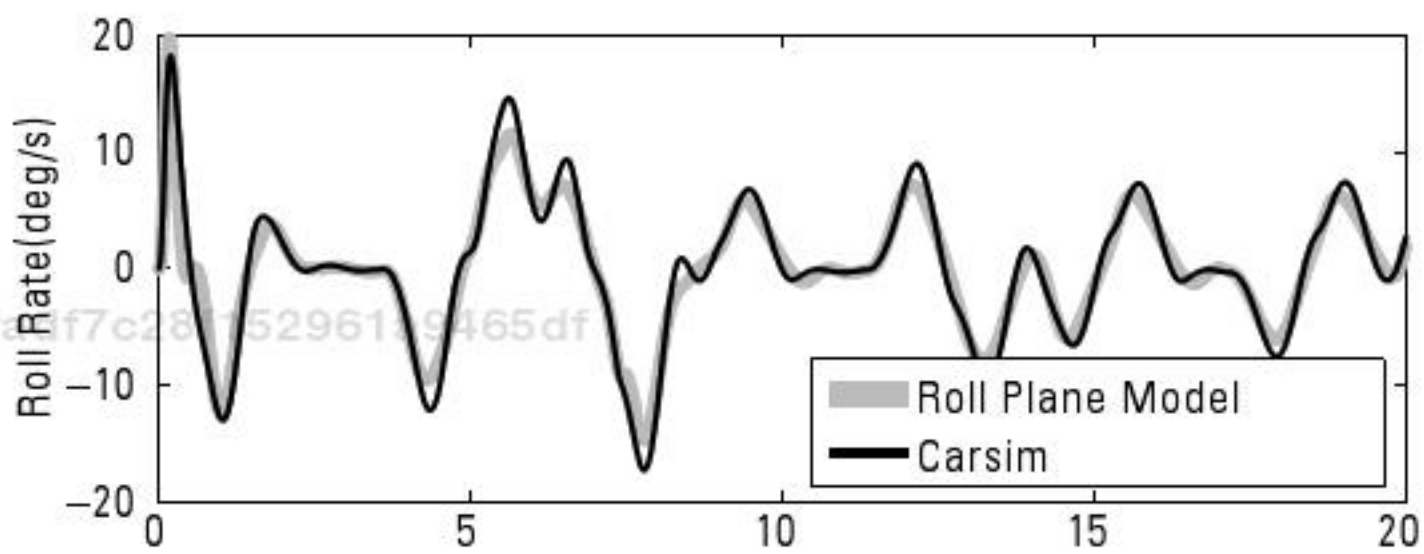

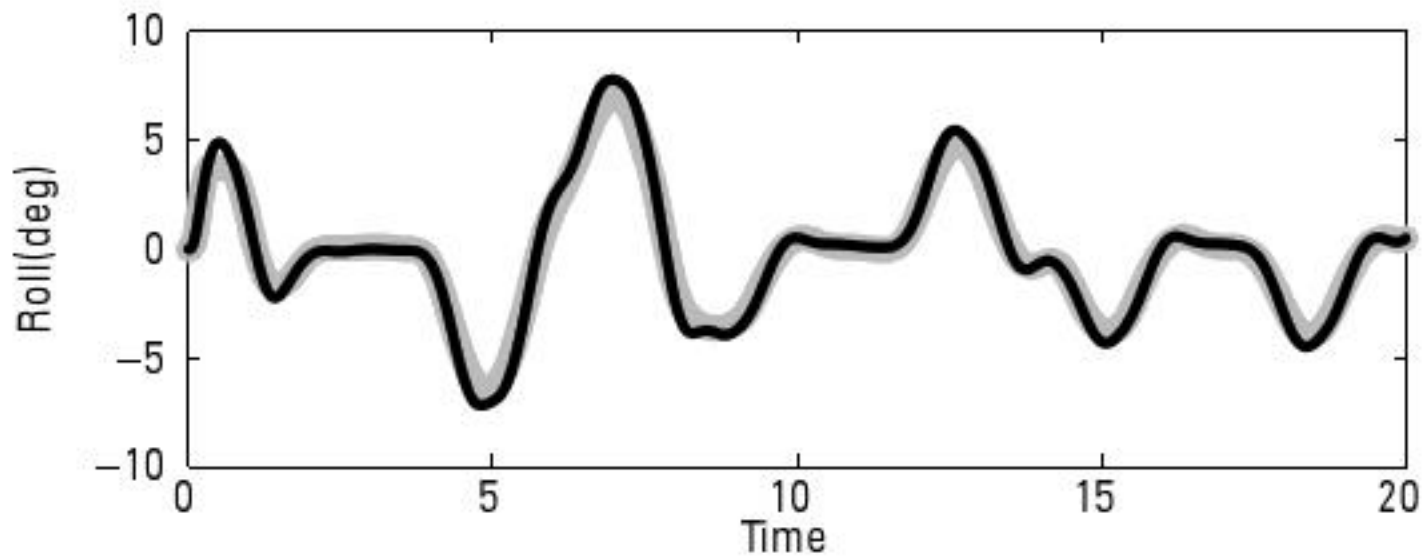

Figure 3.17 Roll plane model validation of a double lane change maneuver in Carsim.

in (3.55), as shown in Figure 3.17. One difference in this model and the Carsim high-fidelity model is the springs used in the Carsim model are highly nonlinear. Shown by (3.54), the simple roll plane model assumes linear springs [9].

You should now have an adequate understanding and introduction to the vehicle models used throughout the proceeding chapters.

References

[1] Milliken, B., and D. Milliken, "Race Car Vehicle Dynamics," *Society of Automotive Engineers*, 1995.

[2] Fiala, E., "Lateral Forces on Rolling Pneumatic Tires," *Zeitschrift,* V. D. I, No. 29:96, 1954.

[3] Pacejka, G. and R. S. Sharp, "Shear Force Development by Pneumatic Tires in Steady State Conditions: A Review of Modelling Aspects," *Vehicle System Dynamics,* Vol. 20, 1991, pp. 121–176.

[4] Pacejka, H. B., E. Bakker, and L. Lidner, "A New Tire Model with an Application in Vehicle Dynamics Studies," SAE Paper, (890087), 1989.

[5] Pacejka, H. B., E. Bakker, and L. Nyborg, "Tyre Modelling for Use in Vehicle Dynamics Studies," SAE Paper, (870421), 1987.

[6] Dugoff, H., P. S. Fancher, and L. Sengal, *Tire Performance Characteristics Affecting Vehicle Response to Steering and Braking Control Inputs*, Technical Report, Office of Vehicle Systems Research, U.S. National Bureau of Standards, 1969.

[7] Pacejka, H. B., and E. Bakker, "The Magic Formula Tyre Model," *Vehicle System Dynamics,* Vol. 21, No. 1, 1992, pp. 1–18.

[8] Ryu, J., "State and Parameter Estimation for Vehicle Dynamics Using GPS," Ph.D. thesis, Stanford University, 2004.

[9] Lambert, K., "A Study of the Properties That Influence Rollover and Their Effect on Electronic Stability Controllers," Master's thesis, Auburn University, 2007.

[10] Rajamani, R., *Vehicle Dynamics and Control,* Springer, 2006.

[11] Whitehead, R. J., "A Study of the Properties That Influence Vehicle Rollover Propensity," Master's thesis, Auburn University, 2005.

[12] Whitehead, R., et al., "A Study of the Effect of Various Vehicle Properties on Rollover Propensity," SAE International, No. 2004-01-2094, Auburn University, 2004.

[13] Solmaz, S., M. Akar, and R. Shorten, "Online Center of Gravity Estimation in Automotive Vehicles using Multiple Models and Switching," *International Conference on Control, Automation, Robotics, and Vision*, 2006.

[14] Solmaz, S., et al., "Realtime Multiple-Model Estimation of Center of Gravity Position in Automotive Vehicles," *Vehicle System Dynamics,* 2007.

[15] Shen, X., J. Dumpert, and S. Farritor, "Design and Control of Robotic Highway Safety Markers," *IEEE/ASME Transactions on Mechatronics,* Vol. 10, No. 5, October 2005.

[16] Gillespie, T. D., "Fundamentals of Vehicle Dynamics," *Society of Automotive Engineers,* 1992.